2 × 2 Textile Rectenna Array with Electromagnetically Coupled Microstrip Patch Antennas in the 2.4 GHz WiFi Band

Juan-Manuel Lopez-Garde [1,*] , Ruben Del-Rio-Ruiz [1] , Jon Legarda [1] and Hendrik Rogier [2]

1 DeustoTech, University of Deusto, Avenida Universidades 24, 48007 Bilbao, Spain; ruben.delrio@deusto.es (R.D.-R.-R.); jlegarda@deusto.es (J.L.)
2 Department of Information Technology, Ghent University-IMEC, Technologiepark Zwijnaarde 126, B-9052 Ghent, Belgium; hendrik.rogier@ugent.be
* Correspondence: jmlopez@deusto.es; Tel.: +34-944419073

Abstract: The development of e-textiles is fostering research in wireless energy transmission. This paper presents a purely textile 2.4 GHz WiFi band 2 × 2 rectenna array for RF energy harvesting. It utilizes the electromagnetically coupled microstrip patch antenna topology and a simple and precise construction method that provides a good performance repeatability to create multilayer microstrip textile patch antennas. The rectifier is implemented with Schottky diodes and it takes the voltage doubling configuration. An average DC power of 1,1 mW was measured for 14 µW/cm^2 of RF input power density, while the end-to-end average power conversion efficiency (PCE) measured was 31%. The characterization of the end-to-end PCE was evaluated considering the physical size of the prototype to make the comparison with other designs easier. Measurements in a real WiFi scenario were also performed, demonstrating its feasibility for feeding e-textiles.

Keywords: energy harvesting; microstrip antennas; rectennas; e-textiles

1. Introduction

The miniaturization of electronics and sensors and their progressive integration, not only in a multitude of wearable devices but also in the garments themselves, is fostering the development of what we call nowadays electronic textiles or e-textiles [1]. There are many and diverse application fields such as medicine [2], sports [3,4], security and defense [5], safety and personal protective equipment (PPE) [6], and even arts and fashion [7,8], which are expectantly awaiting the potential that the combination of these technologies may offer in the future: smart fabrics, wearable electronics and wearable computing.

Collecting, processing and transmitting data, as well as acting on the environment through the electronics embedded in the fabrics, are expected to be the basic functions of e-textiles, which should be aesthetically attractive, lightweight and comfortable, as well as resistant when washed, ironed, bent and wrinkled. The antennas present in these devices are among the main functional components as they can play a triple role. First, they enable connectivity between devices, ensuring efficient data transmission. Secondly, they can be used as presence and movement detection sensors. Finally, they are key for any wireless energy transmission method, both inductive charging and radio frequency energy harvesting (RFEH). Indeed, wireless energy transmission will be a mandatory requirement in many e-textile applications to avoid external connectors and enhance their robustness. For these reasons, this work wants to take a step forward in the design of rectennas.

The rectenna, introduced by Raytheon Co. in 1963 [9], refers to a rectifying antenna that is the first element of an RFEH system. It includes the antenna, which receives the radio waves, and the rectifier, which converts RF power into DC signals. Since their introduction, ambient RFEH systems have been extensively developed [10–12]. Their main challenge is to increase the power conversion efficiency (PCE) due to the small amount of RF energy available in the environment. In outdoor scenarios average exposure levels have been

reported ranging from 84 nW/cm^2 in the GSM1800 band to 0.18 nW/cm^2 in the 2.4 GHz WiFi band [13]. In indoor scenarios average exposure levels of up to 157 nW/cm^2 have been reported for TV/DAB broadcasting and 22 nW/cm^2 in the 2.4 GHz WiFi band [14]. Therefore, RFEH research activities aiming to increase the amount of harvested energy have approached the task using two different strategies [15]. On the one hand, the efficiency of the individual rectenna elements is optimized [16]. On the other hand, antenna array topologies are developed to increase not only the harvested absolute power levels but also the overall efficiency values [17–19]. At this point, it is important to introduce the physical area of the RFEH device in PCE calculations [20,21], as reduction in the size increases the overall calculated PCE.

The use of lightweight, flexible and conformable textile materials opens up great research opportunities in the field of RFEH systems. Table 1 presents the current, most up-to-date and relevant articles related to pure textile rectennas. This shows the operational frequency, the employed textile materials, the construction method, the topology and gain of the antennas, the topology and efficiency of the rectifiers, the array configuration of the rectennas and their overall performance, including their conversion efficiency.

Table 1. Comparison between literature and proposed textile rectennas.

Ref.	Freq. (GHz)	Material		Antenna			Rectifier						Array
		Conductive	Dielectric	Topology	Construction	Gain [1] (dBi)	Topology	Diode	Eff (%)	CE [1] (%)	CE$_{max}$ [1] (%)		Array
[22]	0.9	Nylon Copper Fabric	Jeans	Microstrip	Glue	4.6	Full Wave Bridge	HSMS285X	NA	20	50		NO
[23]	2.45	Silver Ink	PES/ Cotton	Microstrip	Screen printing	NA	Voltage Doubler	NA	NA	NA	NA		NO
[24]	2.45	Polyester Copper Fabric	PES/ Felt	EMCMPA	Glue	8.1	Single	SMS7630	65	NA	29		YES
[21]	2–5	Metallized ink	Cotton	Bowtie	Screen printing	NA	Single	SMS7630	NA	17	32		YES
[25]	2.45	Thread	Organza	Microstrip	Embroidery	6.5	Single	SMS7630	60	NA	NA		YES
Own	2.40–2.48	PCPTF	Felt	EMCMPA	Glue	8.2	Voltage Doubler	SMS7630	56	31	38		YES

[1] Measured value.

In [22] we find one of the first works concerning purely textile rectennas. The materials used are nylon non-woven fabric with copper coating for the conductive layer, and pile and jeans for the substrate layer. It operates in the UHF band (860–918 MHz) and takes a microstrip patch topology, with thin slits to reduce its size and achieve elliptical polarization. For an incident power of 14 μW/cm^2, it achieves a conversion efficiency greater than 20% in the entire band, reaching a maximum of 50% at 876 MHz, and generating approximately 2 mW of DC power. These high power levels are partially obtained due to the greater amount of energy from the emissions of GSM mobile communication systems, usually in outdoor environments.

In [23] a rectenna is shown that is screen printed with silver ink on polycotton. It operates at 2.45 GHz and uses a microstrip patch topology with dual polarization, achieving DC power levels of 100 μW, 15 cm away from a 100 mW PIRE transmitter.

The authors of [24] present the design of a power harvesting wristband. It operates at 2.45 GHz and presents an electromagnetically coupled microstrip patch antenna (EMCMPA) topology. The proposed rectenna obtains DC power from RF input power levels as low as −24.3 dBm by optimizing the design and impedance matching between the antenna and the rectifier. To the best of our knowledge, it is so far the rectenna with the highest sensitivity in literature at 2.45 GHz. The EMCMPA is a purely textile (woven copper plated polyester and felt) antenna; however, the rectifier circuit is implemented on rigid non-textile materials.

The authors of [21] present a purely textile, tightly-coupled rectenna array screen printed on a t-shirt. It works between 2–5 GHz and introduces the physical size in PCE

calculations. It shows two different implementations with 16 and 81 elements, respectively, obtaining an output DC power of 32 μW with 4 μW/cm^2 of incident RF power density. It achieves a maximum efficiency of 32% for high incident power densities, but it comes down to approximately 17% for 14 μW/cm^2 incident power at 2.9 GHz.

Finally, in [25], an array configuration of microstrip patch antennas, made with purely textile materials and embroidered on organza with conductive wires of Cu/Ag50, is presented. It operates in the 2.45 GHz band and reaches a RF-to-DC conversion efficiency of 70% obtained with an input power level of 8 dBm. It achieves DC power levels of 600 μW with a 2 × 3 elements series topology, 10 cm away from the transmitter. It is able to turn-on an LED 60 cm away by supplying 80 μW in boosted WiFi conditions.

Apart from works already included in Table 1, [26,27] present two almost pure textile rectennas working at 0.8 GHz, with peak PCE of up to 63.9% at sub-μW/cm^2 power density levels, providing extremely promising results especially for Wireless Power Transfer (WPT) applications.

This article presents a novel pure textile rectenna design at 2.4 GHz WiFi band. It enhances the performances reported in literature so far based on a combination of the antenna topology, the selection of the textile materials and the fabrication technique. The article is organized as follows: Section 2 describes the design phase of the antenna, the rectifier and their integration. Section 3 shows the test setup and measurements completed for an individual rectenna, while Sections 4 and 5 describe the array configuration and its results, respectively. Finally, conclusions are given in Section 6.

2. Rectenna Design

The novelty of the proposed textile rectenna is based on the combination of the EMCMPA topology [28] and a simple and precise construction method [29] that provides a good performance repeatability for multilayer microstrip textile patch antennas. Thus, the patches and the rectifier circuit pads are laser-cut, and the different layers are attached with double-sided, thermally activated adhesive sheets. This section comprises three phases: firstly, the design of the antenna, secondly the design of the rectifier and finally the integration of both.

2.1. Antenna Design

The EMCMPA topology, in addition to being planar, has a non-contact configuration between the feed line and radiating patch [28]. Because of this, it is optimal for textile rectennas as the feeding line and rectifying stage coincide in the same layer, avoiding additional soldering points and therefore increasing its overall flexibility. The electromagnetically coupled radiating patch also helps obtain an independent EM optimization of the feeding mechanism and patch, decreasing the overall antenna dimensions without altering their EM performance. In addition to this, the construction process [29] shows very good agreement between simulation and measurements, and the standard deviation of measured resonant frequencies, impedance bandwidths, gains and total efficiencies equal 24.54 MHz, 14.02 MHz, 0.15 dBi and 3.57%, respectively.

The chosen textile materials are 80 μm thick pure copper polyester taffeta fabric (PCPTF) and 1.2 mm thick felt, for the conductive and dielectric layers, respectively. PCPTF is a plain woven fabric, coated with pure copper, with a low surface resistivity of 0.05 Ω/sq at 2.45 GHz, and an approximate weight of 80 g/m^2, making it suitable for the construction of textile EMCMPA. Felt, on the other hand, has a permittivity ε' and loss tangent $tan\delta$ at 2.45 GHz of 1.25 and 0.003, respectively.

The designed EMCMPA is composed (top to bottom) of a radiating patch ($W_p \times L_p$), a dielectric layer ($W_{sub} \times L_{sub}$), a feed line ($W_{line} \times L_{line}$), a second dielectric layer ($W_{sub} \times L_{sub}$) and a ground layer ($W_g \times L_g$), as shown in Figure 1. The antenna's overall assembly comprises three conductive layers with a thickness of h_{cond} each, and two dielectric layers with a thickness of h_{sub} each. The antenna dimensions are listed in Table 2.
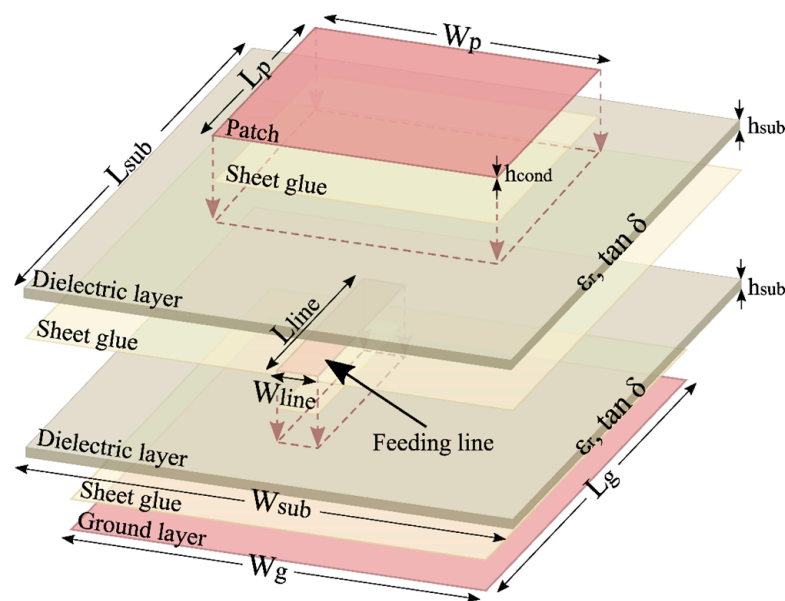
Figure 1. Perspective view of the electromagnetically coupled microstrip patch textile antenna structure. For clarity, all the antenna layers have been separated and labeled at the side.

Table 2. Proposed antenna dimensions [1].

| W_p	L_p	W_g	L_g	W_{sub}	L_{sub}	W_{line}	L_{line}
57.96	51.10	72.36	65.50	84.36	77.50	10.4	27.75

[1] Units: mm.

The EMCMPA is excited by a microstrip feed line, which is electromagnetically coupled through the top substrate to the radiating patch. The feed line is located between the ground layer and the radiating patch such that any radiation from the feed line is shielded and potentially re-radiated by the patch, leading to a good cross-polarization [30]. This topology places the radiating patch further away from the ground plane, which leads to enhanced bandwidth and efficiency values. The antenna design is computer aided using the CST Studio Suite, obtaining an input impedance Z_{in} of 49.21-j2.78 Ω at 2.44 GHz.

The antenna characterization is performed in an anechoic chamber with an Agilent N5242A PNA-X Microwave Network Analyzer. The reflection coefficient and radiation patterns in free space are shown in Figures 2 and 3, respectively, where a good agreement between measured and simulated values is observed. The return loss amplitude difference in the antenna's resonance frequency is up to 15 dB due to the handmade SMA connectorization and inhomogeneities in the substrate's dielectric properties, which are in agreement with values found in literature [31–33]. Yet, simulated and measured S_{11} results remain under −10 dB across the whole 2.4 GHz WiFi band. As it can be observed in Figure 4, at 2.45 GHz the simulated and measured gain is 8.7 dBi and 8.2 dBi, respectively, while the simulated and measured radiation efficiency is 76% and 85%. The difference observed in the efficiency could be due to the inhomogeneities of the textile substrate, as well as the overestimation of the *tanδ* parameter in simulation.
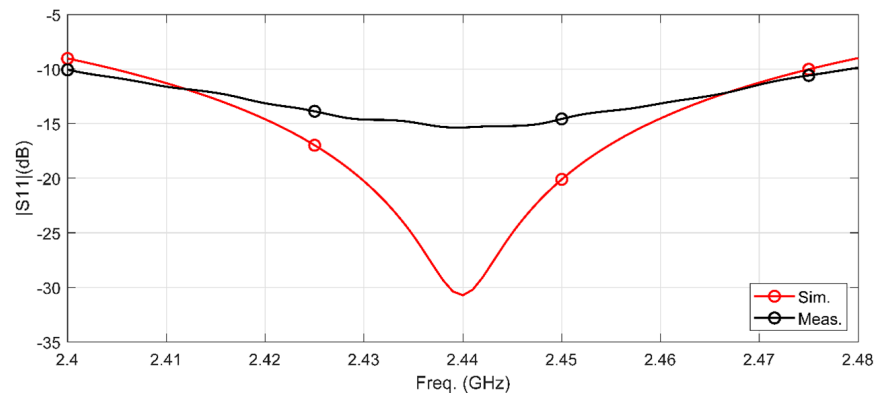
Figure 2. Electromagnetically coupled microstrip patch antenna's simulated and measured reflection coefficient in free-space.
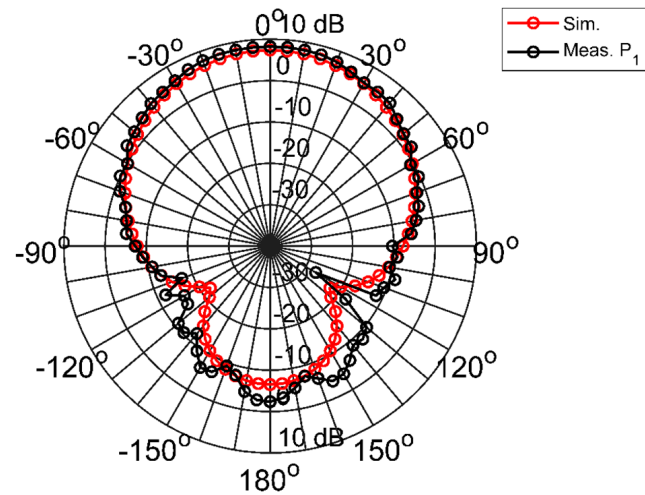
Figure 3. Electromagnetically coupled microstrip patch antenna's simulated and measured radiation patterns in free-space at 2.45 GHz.
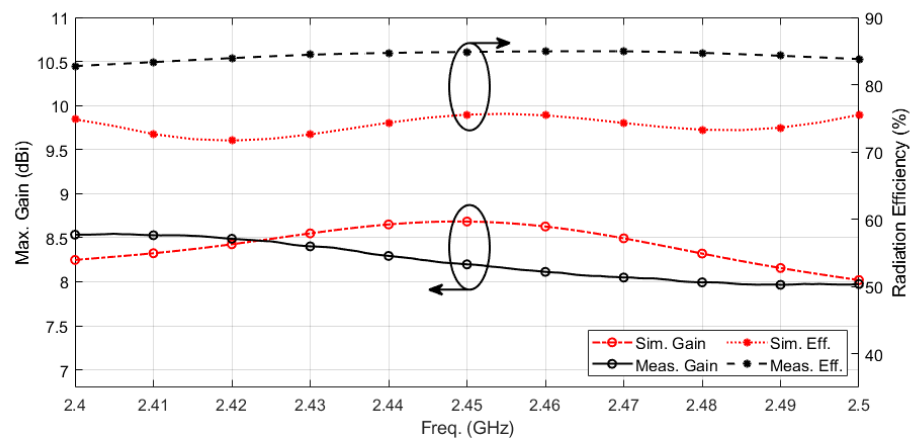
Figure 4. Electromagnetically coupled microstrip patch antenna's simulated and measured Gain and Radiation Efficiency.

2.2. Rectifier Design

RFEH systems deal with very low-power signal levels [13,14], therefore, Schottky diodes are a good choice for the rectifier due to their fast switching time, low threshold voltage, exponential voltage drop with current, and stable performance with temperature [12,34]. In this work, -3 dBm and 0 dBm RF input power levels are used at the

rectifier stage to guarantee that the Schottky diodes operate properly. These input power levels are realistic values in the vicinity of commercial WiFi access points where maximum transmitting power is limited to +20 dBm.

The rectifier is based on the SMS7630 diode from Skyworks. Its surface mount package allows its use in textile designs. A full-wave rectifier is preferable [10] to increase RF-to-DC power conversion and a minimum number of components is desirable to reduce textile integration complexity. Therefore, a rectifying configuration that copes with both requirements is the voltage doubling circuit, with only two diodes and two capacitors, as shown in Figure 5. The output voltage V_{DC} doubles the input voltage V_{peak}, with both capacitors in series. It is a stable and efficient scheme that avoids the use of DC-DC converters to raise the output voltage.
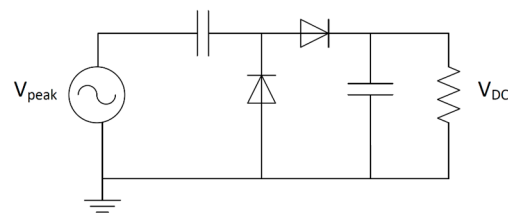

Figure 5. Voltage doubling circuit.

The rectifier has been designed with the computer-aided Keysight ADS. The packaging of each diode and the parasitic effects of the soldering have been characterized with two equal inductances in series and a capacitance in parallel (2.87 nH and 0.37 pF respectively). Similarly, 1 mm long transmission lines have been included to simulate the soldering points of the lumped elements onto the PCPTF. As in the case of the antenna, the rectifier has been built with PCPTF and felt, as shown in Figure 6.
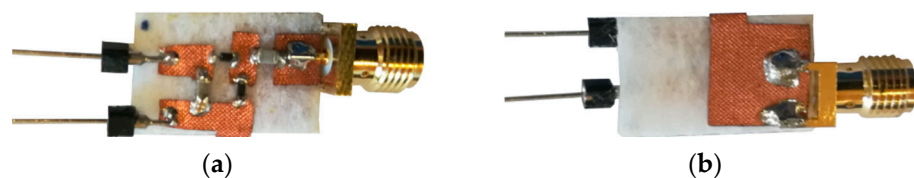

(**a**)   (**b**)

Figure 6. Textile rectifier: (**a**) Top layer; (**b**) Bottom layer.

To reduce the inherent lab-scale construction uncertainty of the textile rectifiers, measurements have been carried out on four different prototypes and the average values of the DC output voltage have been calculated. Figure 7 shows the output V_{DC} values on a 1K6 resistor for different input power levels P_{IN} at 2.45 GHz, with a good concordance between measured and simulated results.
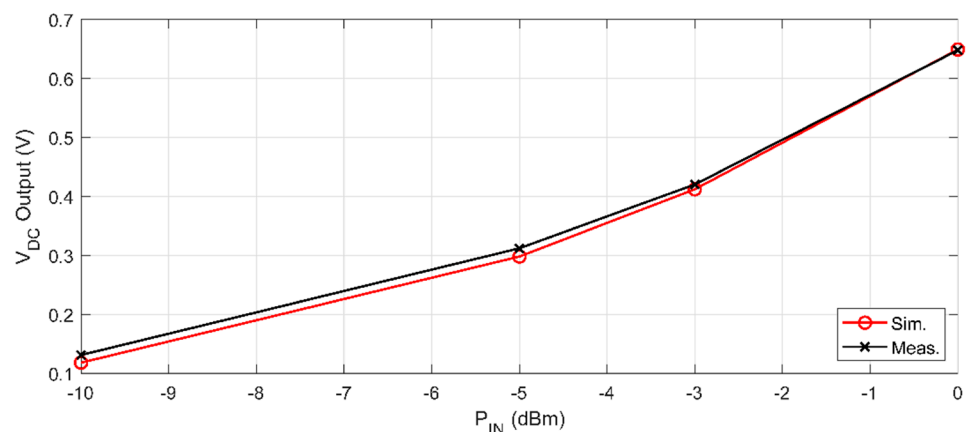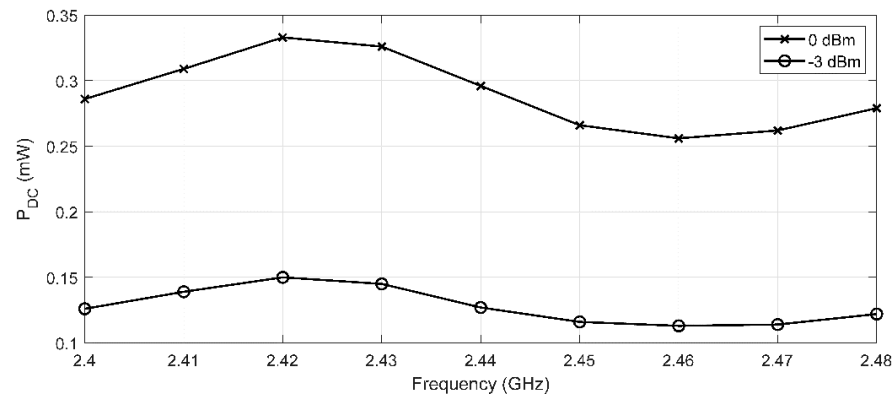

Figure 7. Textile rectifier output V_{DC} vs. input power P_{IN} (2.45 GHz).

On the other hand, Figure 8 shows P_{DC} values vs. frequency measured at the rectifier output for the two different input power levels (0 and -3 dBm). Maximum values of 0.33 mW and 0.15 mW are obtained at 2.42 GHz, while the average values observed in the whole 2.4 GHz WiFi band are 0.29 mW and 0.13 mW, respectively.


Figure 8. Textile rectifier output DC power P_{DC} vs. Frequency.

2.3. Rectenna Integration

The impedance matching network between the antenna and the rectifier is critical to increase the PCE. The input impedance of the rectifier depends not only on the frequency of the input signal but also on its power level, which is extremely complex to predict since it depends on the instantaneous RF signal present in the environment. This non-linearity of the input impedance of the rectifier leads to the utilization of a different method to calculate the matching network to maximize the energy transmission from the antenna to the rectifier.

The matching network has been calculated so that it maximizes the DC output voltage of the rectifier. The input power levels are swept between -3 dBm and 0 dBm at the output of the antenna. Moreover, to reduce the number of discrete components and the number of soldering points, distributed elements are used instead of lumped elements. The resultant matching network consists of a 7.53 mm long transmission line and a 14.01 mm long open circuit stub in parallel.

Figure 9 shows the dielectric bottom layer, including EMCMPA feeding line, the matching network and the rectifier layout.
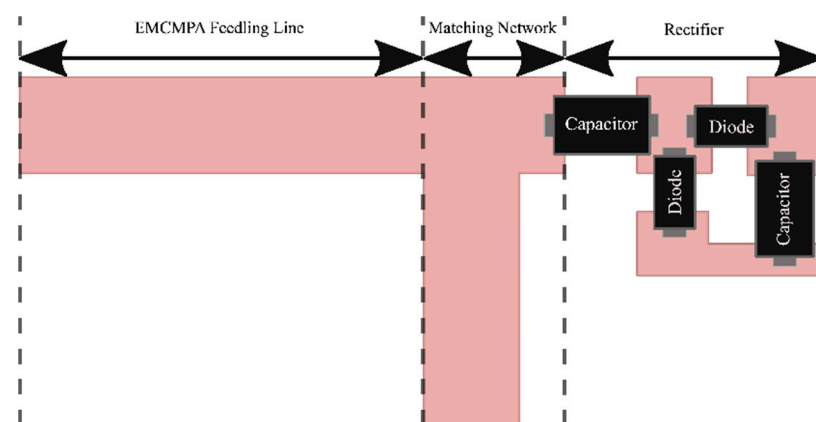
Figure 9. Electromagnetically coupled microstrip patch feeding line, matching network and rectifier layout.

Figure 10 shows a perspective view of the rectenna construction process with all the layers from top to bottom: EMCMPA patch, top dielectric layer, rectifier layer (including matching network and EMCMPA feeding line), bottom dielectric layer and ground plane.
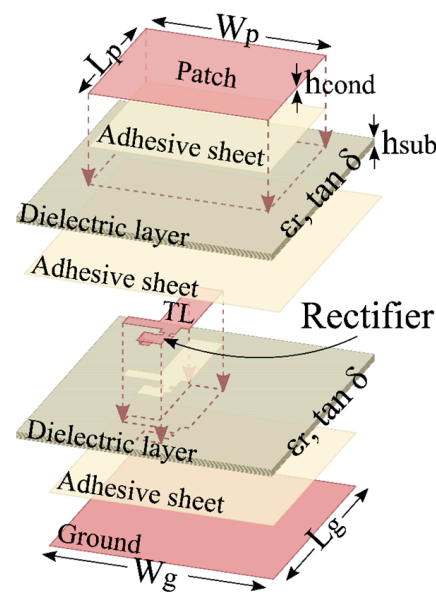
Figure 10. Perspective view of textile rectenna.

3. Single Rectenna Measurements

This section describes the test setup used for the characterization of the PCE of the rectenna shown in Section 2.3. The PCE is defined according to

$$PCE = \frac{P_{DC}}{\wp_{RX}\cdot A} \tag{1}$$

where A is the rectenna physical area, $\wp_{RX}$ is the power density of the incident plane wave and P_{DC} is the DC power obtained at the 1K6 load resistor located at the rectenna output.

The correct characterization of the rectenna requires a well-known power level P_{RX} at the input of the rectifier stage to ensure that the obtained results for the rectifier alone can be properly compared with those obtained for the whole rectenna. This is performed in two phases: first, the rectifier input power is configured and, second, the rectenna PCE is measured.

3.1. Rectifier Input Power Configuration

The rectifier's input power P_{RX} is set between 0 dBm and −3 dBm, as stated in Section 2.2. Figure 11 shows the setup deployed to achieve these power levels at the desired 2.4 GHz WiFi band. It is composed of an Agilent E4433B Signal Generator, an Agilent N9030A PXA Signal Analyzer and two well characterized textile EMCMPA antennas, identical to the one present in the rectenna.

Figure 11. P_{RX} configuration test setup.

The signal generator is configured to provide +12 dBm to the transmitting antenna. The average measured power in the 2.4 GHz WiFi frequency band at the terminal of the receiving antenna, and the power density $\wp$ ($\mu W/cm^2$) of the incident plane wave in the receiving antenna, are shown in Table 3. The latter has been calculated by means of the Friis transmission equation

$$\wp_{RX} = P_{TX}\cdot\left(1 - |S_{11}|^2\right)\cdot G\cdot\frac{1}{4\pi d^2} \tag{2}$$

considering the measured gain G and reflection coefficient S_{11} of the EMCMPA antennas at each frequency. The separation distance between antennas d is determined when the output power at the receiving antenna is 0 dBm.

**Table 3.** P_{RX} configuration values.

P_{TX} (dBm)	G (dBi)	S_{11} (dB)	$\wp_{RX}$ (µW/cm^2)	P_{RX} (dBm)	*Distance* (m)
+12	7.8	−12.6	14	+0	0.21

3.2. Individual Rectenna PCE Measurements

After determining the separation distance d and considering that it falls into the far-field region, the receiving side of the test setup is replaced by the rectenna, and the signal analyzer is replaced by an Agilent N6705B DC Power Analyzer, as shown in Figures 12 and 13.
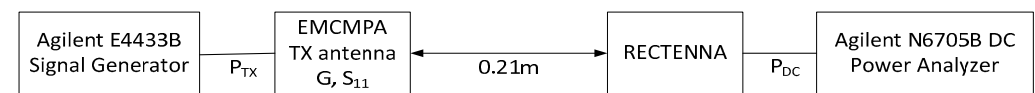
Figure 12. PCE measurement test setup.
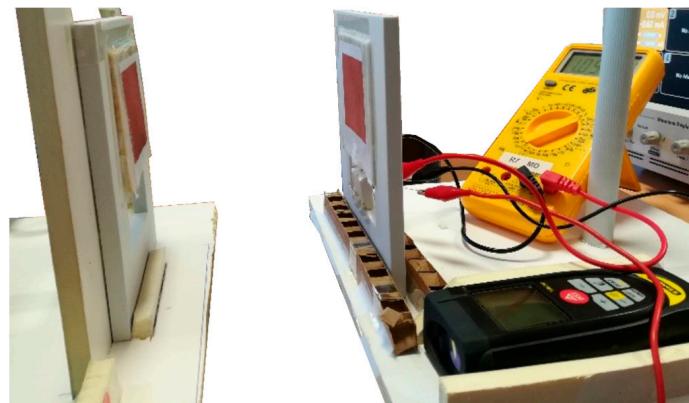
Figure 13. Single rectenna PCE measurement setup.

V_{DC} and I_{DC} values are measured in a 1K6 load resistor so that P_{DC} can be calculated accordingly. Table 4 shows P_{DC} maximum and P_{DC} average values in the 2.4 GHz WiFi band for two different input power levels. PCE is also calculated according to eq (1), taking into account rectenna actual dimensions (7.2 × 8 cm^2).

Table 4. Rectenna measured values (2.40–2.48 GHz Band).

P_{TX} (dBm)	$\wp_{RXavg}$ (µW/cm^2)	P_{DCmax} (mW)	P_{DCavg} (mW)	PCE_{max} (%)	PCE_{avg} (%)
+9	7	0.087	0.072	26	19
+12	14	0.261	0.207	38	29

Figure 14 shows that for the same input power, rectenna P_{DC} is lower: the values measured are 71% and 55% of values obtained by the rectifier alone for 0 dBm and −3 dBm P_{RX} input power, respectively.
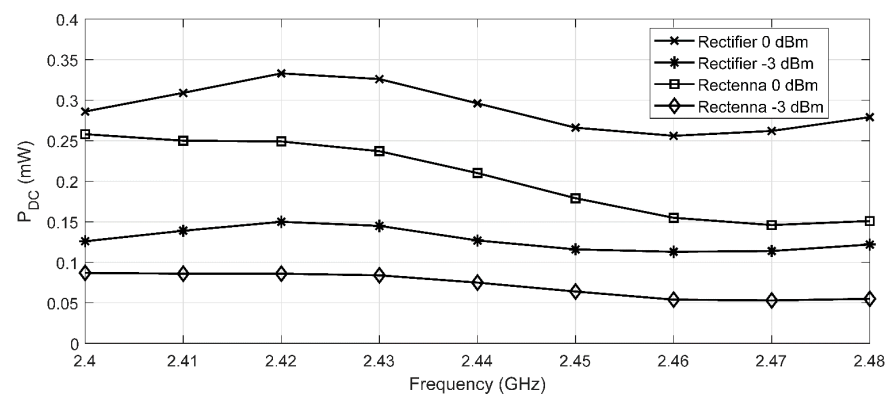
Figure 14. Rectifier vs. Rectenna output DC power P_{DC} comparison.

4. Rectenna Array Configuration

The array configuration of several rectennas is considered to increase the capacity to harvest energy. The RF combination of signals coming from each antenna prior to reaching a single rectifying stage achieves higher directivities, it needs fewer components and utilizes the diodes more efficiently as they receive higher power levels [17]. However, in order to harvest energy coming from a wider beam, the signal coming from each antenna is rectified individually and combined at DC stage. According to [35], the parallel-connection topology for the rectifiers has higher overall efficiency than the series-topology rectifier, except when rectifiers deal with the same amount of power, where the series-topology efficiency is slightly higher. Considering that all of the antennas receive the same amount of radiated power density, in this work, a topology with four rectennas connected in series has been chosen in order to obtain higher voltage levels.

The spacing of the elements is the key design parameter of the array. The criteria taken into consideration have been doubled. On the one hand, this is to minimize the size of the system and, on the other hand, to guarantee the absence of coupling between the antenna elements to avoid their performance degradation. Thus, after a computer aided optimization process in CST, the 2 × 2 array configuration was chosen, as shown in Figure 15, where the horizontal and vertical spacing between antenna patches is dW (8.2 mm) and dL (10.5 mm), respectively. Efficiency and gain values obtained for each antenna element of the array do not differ from those obtained for the individual element alone, while the uncoupling between individual patches is higher than 25 dB.
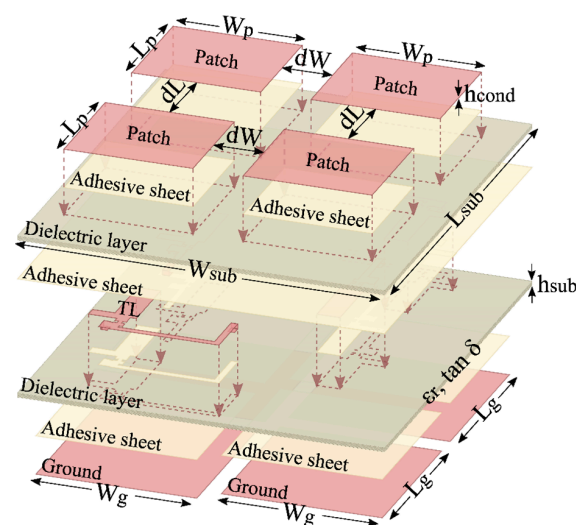

Figure 15. Proposed 2 × 2 rectenna array configuration. For clarity, all the antenna layers have been separated and labeled at the side.

The array construction process is illustrated in Figure 16, where the rectenna layers are shown together with the wooden frames used for their correct alignment [29]. Starting with the ground plane, (a) shows its placement on the bottom dielectric layer that can be seen in (b) after turning it around. In (c) and (d) the assembly process of the third layer is illustrated including the rectifiers, the matching networks and the patch feed lines. The serial connection of the rectennas is made by means of lines going through this intermediate layer and textile vias that connect it to the ground plane. This can be observed in the enlarged areas, together with the position of the rectifiers' components. Finally, (e) shows the placement of the top dielectric layer and the patch antennas, while the final prototype top view is presented in (f).
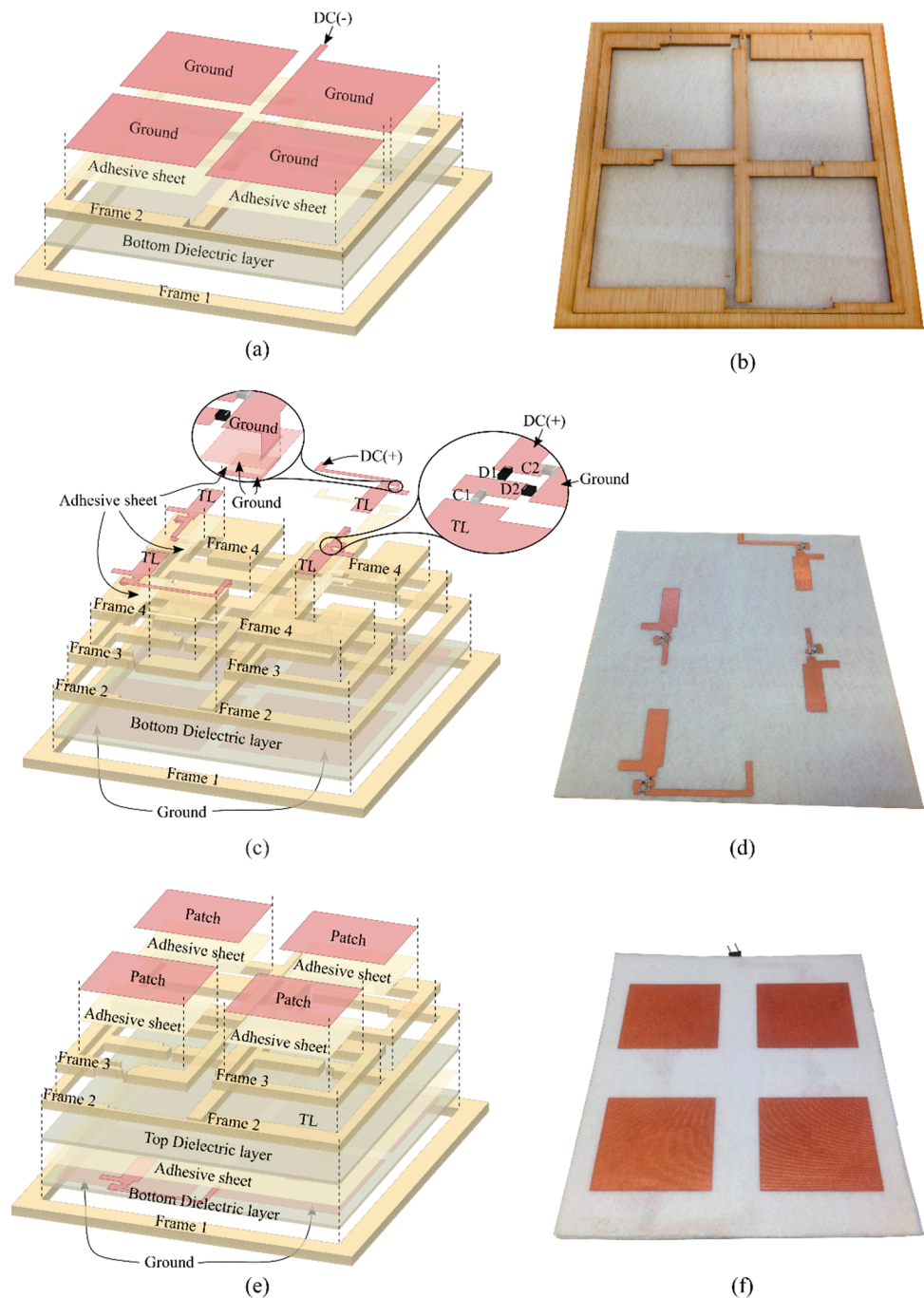
Figure 16. Rectenna construction process. For clarity, all the antenna layers have been separated and labeled at the side.

5. Array Measurements

Array measurements were completed using the same test setup previously shown in Figure 13. A perfect alignment between the transmitting antenna and the array of rectennas is required to ensure that each individual element receives the same RF power density.

The average DC power measured in the 2.4 GHz WiFi band for 14 µW/cm^2 of RF input power density was 1,1 mW, while the end-to-end average PCE measured was 31%. Comparing the results with those obtained for the single rectenna, it can be observed that the measured PCE was maintained; while single rectenna showed average PCEs of 29% and 19% for 0 dBm and −3 dBm, respectively, the 2 × 2 array provided average PCE values of 31% and 21%. These results prove the scalability of the design: the array series connection of individual rectenna elements makes it possible to increase the amount of harvested energy.

On-body performance of the EMCMPA is verified in [28], with good agreement between simulation and measurement. In order to verify that rectenna configuration maintains the on-body performance, new measurements were made, as shown in Figure 17. P_{DC} values measured in the 2.4 GHz WiFi band for both input power levels are shown in Figure 18. Tables 5 and 6 summarize the PCE performance comparison of a 15 × 18 cm^2 rectenna array. The obtained rectenna array results had good agreement in both free-space and on-body measurements, which indicates that most of the incident radiation is received by the EMCMPA owing to the presence of a ground plane and a shielded feed line, therefore providing a good rectenna-body isolation.
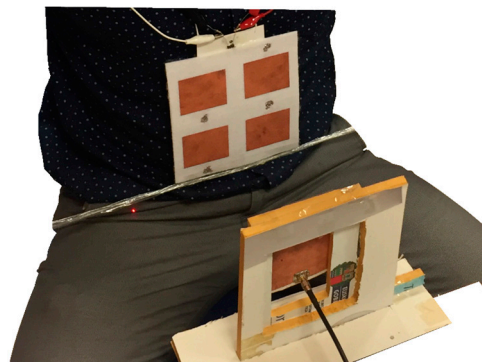

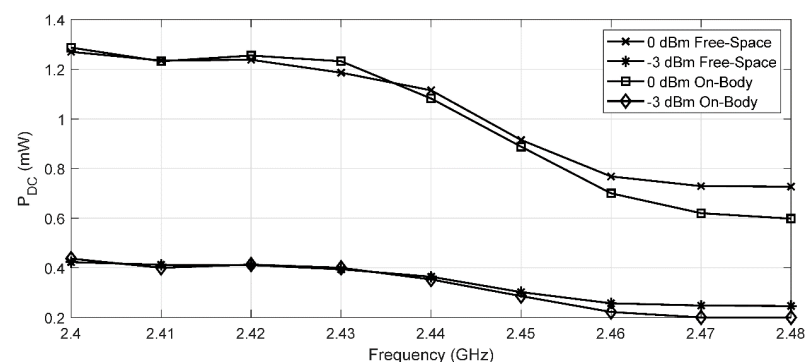**Figure 17.** On-body measurement setup.

Figure 18. 2 × 2 rectenna output DC power P_{DC} vs. frequency measurements in free-space and on-body.

Table 5. 2 × 2 Rectenna Array Measurements (2.40–2.48 GHz Band).

P_{TX} (dBm)	$\wp_{RXavg}$ (μW/cm^2)	P_{DCmax} (mW)	P_{DCavg} (mW)	PCE_{max} (%)	PCE_{avg} (%)
+9	7	0.431	0.358	26	21
+12	14	1.281	1.068	38	31

Table 6. 2 × 2 Rectenna Array On-body Measurements (2.40–2.48 GHz Band).

| P_{TX} (dBm)	$\wp_{RXavg}$ (μW/cm^2)	P_{DCmax} (mW)	P_{DCavg} (mW)	PCE_{max} (%)	PCE_{avg} (%)
+9	7	0.437	0.323	27	19
+12	14	1.287	0.988	40	29

Additional measurements were performed to obtain results in a more realistic application scenario. On the one hand, measurements were taken for a lower transmission power level (+6 dBm/3,5 μW/cm^2), and two different orientations (30° and 45°) were tested, in order to check the rectenna performance at lower power levels. Results in Table 7 show that the performance degradation observed agrees with the patches gain reduction at different angles, together with the rectifier efficiency decrease at these lower power levels. On the other hand, the 2 × 2 rectenna array was placed in front of a commercial WiFi access point, as shown in Figure 19, transmitting at its maximum allowed indoors PIRE of 100 mW (+20 dBm). The average P_{DC} measured in the 2.4 GHz WiFi band was 0.503 mW at a distance of 0.21 m, the point where −3 dBm was obtained by the EMCMPA from a WiFi access point equipped with omnidirectional antennas transmitting at 100 mW (+20 dBm). In this case, and because of the omnidirectional pattern of the WiFi access point, its orientation with respect to the rectenna array did not change the amount of power obtained.

Table 7. 2 × 2 Rectenna Array Measurements (2.40–2.48 GHz Band).

P_{TX} (dBm)	$\wp_{RXavg}$ (μW/cm^2)	Angle (°)	P_{DCmax} (mW)	P_{DCavg} (mW)	PCE_{max} (%)	PCE_{avg} (%)
+12	14	0	1.281	1.068	0.38	0.31
		30	0.888	0.703	0.26	0.20
		45	0.460	0.350	0.14	0.10
+9	7	0	0.431	0.358	0.26	0.21
		30	0.275	0.220	0.17	0.13
		45	0.126	0.097	0.08	0.06
+6	3.5	9	0.154	0.125	0.19	0.14
		30	0.088	0.070	0.11	0.08
		45	0.036	0.027	0.04	0.03

The results obtained in this work are promising, in comparison to the latest literature found on fully textile rectennas for the 2.4 GHz WiFi band. In [25] a similar embroidered textile 2 × 2 rectenna array configuration is presented, under equivalent ambient WiFi signals, providing around 0.100 mW at the same distance of 0.21 m, while our work provides 0.503 mW, five times more power. In addition, if the rectennas' sizes are taken into consideration, our design is 10% smaller, providing a better overall PCE. In the same way, in [21] a screen-printed textile 16 × 16 array reports a 17% PCE while our design obtains 31% for the same RF input power density.
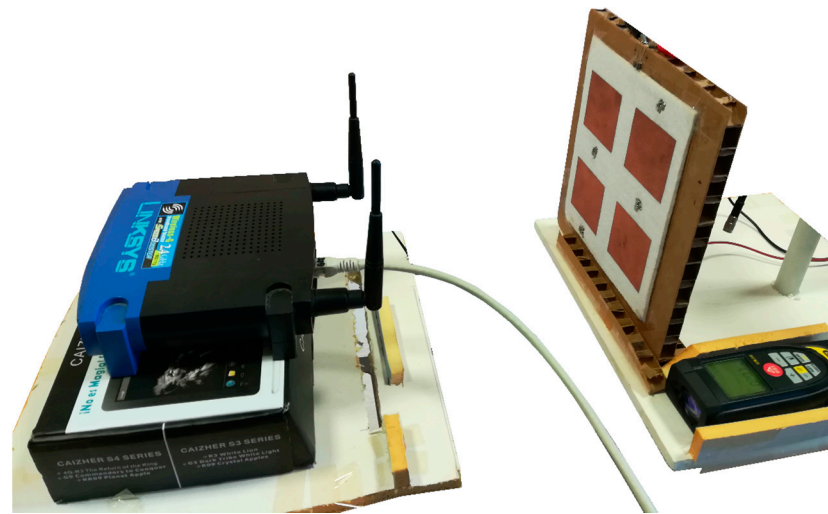
Figure 19. WiFi access point measurement.

6. Conclusions

A fully textile rectenna has been designed, constructed and validated. The combination of the EMCMPA topology and a simple and precise construction method has led to better results than those reported in literature: the average DC power measured in the 2.4 GHz WiFi band for 14 μW/cm^2 of RF input power density was 1,1 mW, while the end-to-end average PCE measured was 31%. The characterization of the end-to-end PCE has been completed considering the physical size of the prototype to make comparison with other designs easier. On-body measurements have shown a good rectenna-body isolation, and the scalability of the design has been proven by verifying that the 2×2 array configuration maintains efficiency while the amount of harvested energy is increased.

Author Contributions: J.-M.L.-G. contributed to the conceptualization, investigation, resources, and the overall research. R.D.-R.-R. contributed to the investigation, resources, writing—review and editing. J.L. contributed to the writing—review and editing, supervision and project administration. H.R. contributed to the writing—review and editing. All authors have read and agreed to the published version of the manuscript.

Conflicts of Interest: The authors declare no conflict of interest. The funders had no role in the design of the study; in the collection, analyses, or interpretation of data; in the writing of the manuscript, or in the decision to publish the results.

References

1. Stoppa, M.; Chiolerio, A. Wearable Electronics and Smart Textiles: A Critical Review. *Sensors* **2014**, *14*. [CrossRef] [PubMed]
2. Yang, K.; Isaia, B.; Brown, L.J.E.; Beeby, S. E-Textiles for Healthy Ageing. *Sensors* **2019**, *19*, 4463. [CrossRef]
3. Feito, Y.; Moriarty, T.A.; Mangine, G.; Monahan, J. The use of a smart-textile garment during high-intensity functional training: A pilot study. *J. Sports Med. Phys. Fit.* **2019**, *59*, 947–954. [CrossRef] [PubMed]
4. Schmitz, B.; Hofmann, C.; Maestre, R.; Bleda, A.L.; Tobola, A.; Melcher, V.; van Gent, J. Continuous vital monitoring and automated alert message generation for motorbike riders. In Proceedings of the 2015 Computing in Cardiology Conference (CinC), Nice, France, 6–9 September 2015; pp. 397–400.
5. Nayak, R.; Wang, L.; Padhye, R. 11—Electronic textiles for military personnel. In *Electronic Textiles*; Dias, T., Ed.; Woodhead Publishing: Oxford, UK, 2015; pp. 239–256.
6. Chen, D.; Lawo, M. Smart Textiles and Smart Personnel Protective Equipment. In *Smart Textiles: Fundamentals, Design, and Interaction*; Schneegass, S., Amft, O., Eds.; Springer International Publishing: Cham, Switzerland, 2017; pp. 333–357.

7. Peppler, K. STEAM-Powered Computing Education: Using E-Textiles to Integrate the Arts and STEM. *Computer* **2013**, *46*, 38–43. [CrossRef]
8. Jaquard by Google Weaves New Digital Experiences into the Things You Love, Wear, and Use Every Day to Give You the Power to Do More and Be More. Available online: https://atap.google.com/jacquard/ (accessed on 22 January 2020).
9. Brown, W.C. The History of Power Transmission by Radio Waves. *IEEE Trans. Microw. Theory Tech.* **1984**, *32*, 1230–1242. [CrossRef]
10. Tran, L.-G.; Cha, H.-K.; Park, W.-T. RF power harvesting: A review on designing methodologies and applications. *Micro Nano Syst. Lett.* **2017**, *5*, 14. [CrossRef]
11. Visser, H.J.; Vullers, R.J.M. RF Energy Harvesting and Transport for Wireless Sensor Network Applications: Principles and Requirements. *Proc. IEEE* **2013**, *101*, 1410–1423. [CrossRef]
12. Soyata, T.; Copeland, L.; Heinzelman, W. RF Energy Harvesting for Embedded Systems: A Survey of Tradeoffs and Methodology. *IEEE Circuits Syst. Mag.* **2016**, *16*, 22–57. [CrossRef]
13. Piñuela, M.; Mitcheson, P.D.; Lucyszyn, S. Ambient RF Energy Harvesting in Urban and Semi-Urban Environments. *IEEE Trans. Microw. Theory Tech.* **2013**, *61*, 2715–2726. [CrossRef]
14. Chiaramello, E.; Bonato, M.; Fiocchi, S.; Tognola, G.; Parazzini, M.; Ravazzani, P.; Wiart, J. Radio Frequency Electromagnetic Fields Exposure Assessment in Indoor Environments: A Review. *Int. J. Environ. Res. Public Health* **2019**, *16*, 955. [CrossRef]
15. Carvalho, N.B.; Georgiadis, A.; Costanzo, A.; Rogier, H.; Collado, A.; García, J.A.; Lucyszyn, S.; Mezzanotte, P.; Kracek, J.; Masotti, D.; et al. Wireless Power Transmission: R&D Activities within Europe. *IEEE Trans. Microw. Theory Tech.* **2014**, *62*, 1031–1045. [CrossRef]
16. Valenta, C.R.; Durgin, G.D. Harvesting Wireless Power: Survey of Energy-Harvester Conversion Efficiency in Far-Field, Wireless Power Transfer Systems. *IEEE Microw. Mag.* **2014**, *15*, 108–120. [CrossRef]
17. Olgun, U.; Chen, C.; Volakis, J.L. Investigation of Rectenna Array Configurations for Enhanced RF Power Harvesting. *IEEE Antennas Wirel. Propag. Lett.* **2011**, *10*, 262–265. [CrossRef]
18. Khang, S.; Lee, D.; Hwang, I.; Yeo, T.; Yu, J. Microwave Power Transfer with Optimal Number of Rectenna Arrays for Midrange Applications. *IEEE Antennas Wirel. Propag. Lett.* **2018**, *17*, 155–159. [CrossRef]
19. Popović, Z.; Korhummel, S.; Dunbar, S.; Scheeler, R.; Dolgov, A.; Zane, R.; Falkenstein, E.; Hagerty, J. Scalable RF Energy Harvesting. *IEEE Trans. Microw. Theory Tech.* **2014**, *62*, 1046–1056. [CrossRef]
20. Chuma, E.L.; Rodríguez, L.d.l.T.; Iano, Y.; Roger, L.L.B.; Sanchez-Soriano, M.-A. Compact rectenna based on a fractal geometry with a high conversion energy efficiency per area. *IET Microw. Antennas Propag.* **2018**, *12*, 173–178. [CrossRef]
21. Estrada, J.A.; Kwiatkowski, E.; López-Yela, A.; Borgoñós-García, M.; Segovia-Vargas, D.; Barton, T.; Popović, Z. RF-Harvesting Tightly Coupled Rectenna Array Tee-Shirt with Greater than Octave Bandwidth. *IEEE Trans. Microw. Theory Tech.* **2020**, *68*, 3908–3919. [CrossRef]
22. Monti, G.; Corchia, L.; Tarricone, L. UHF Wearable Rectenna on Textile Materials. *IEEE Trans. Antennas Propag.* **2013**, *61*, 3869–3873. [CrossRef]
23. Adami, S.; Zhu, D.; Yi, L.; Mellios, E.; Stark, B.H.; Beeby, S. A 2.45 GHz rectenna screen-printed on polycotton for on-body RF power transfer and harvesting. In Proceedings of the 2015 IEEE Wireless Power Transfer Conference (WPTC), Boulder, CO, USA, 13–15 May 2015; pp. 1–4.
24. Adami, S.E.; Proynov, P.; Hilton, G.S.; Yang, G.; Zhang, C.; Zhu, D.; Li, Y.; Beeby, S.P.; Craddock, I.J.; Stark, B.H. A Flexible 2.45-GHz Power Harvesting Wristband with Net System Output from −24.3 dBm of RF Power. *IEEE Trans. Microw. Theory Tech.* **2018**, *66*, 380–395. [CrossRef]
25. Vital, D.; Bhardwaj, S.; Volakis, J.L. Textile-Based Large Area RF-Power Harvesting System for Wearable Applications. *IEEE Trans. Antennas Propag.* **2020**, *68*, 2323–2331. [CrossRef]
26. Wagih, M.; Weddell, A.S.; Beeby, S. Omnidirectional Dual-Polarized Low-Profile Textile Rectenna with Over 50% Efficiency for Sub-μW/cm^2 Wearable Power Harvesting. *IEEE Trans. Antennas Propag.* **2021**, *69*, 2522–2536. [CrossRef]
27. Wagih, M.; Hilton, G.S.; Weddell, A.S.; Beeby, S. Dual-Band Dual-Mode Textile Antenna/Rectenna for Simultaneous Wireless Information and Power Transfer (SWIPT). *IEEE Trans. Antennas Propag.* **2021**, 1. [CrossRef]
28. Del-Rio-Ruiz, R.; Lopez-Garde, J.M.; Legarda, J.; Caytan, O.; Rogier, H. A Combination of Transmission Line Models as Design Instruments for Electromagnetically Coupled Microstrip Patch Antennas in the 2.45 GHz ISM Band. *IEEE Trans. Antennas Propag.* **2021**, *69*, 550–555. [CrossRef]
29. Del-Rio-Ruiz, R.; Lopez-Garde, J.; Legarda, J.; Lemey, S.; Caytan, O.; Rogier, H. Reliable Lab-Scale Construction Process for Electromagnetically Coupled Textile Microstrip Patch Antennas for the 2.45 GHz ISM Band. *IEEE Antennas Wirel. Propag. Lett.* **2020**, *19*, 153–157. [CrossRef]
30. Duffy, S.M. An enhanced bandwidth design technique for electromagnetically coupled microstrip antennas. *IEEE Trans. Antennas Propag.* **2000**, *48*, 161–164. [CrossRef]
31. Soh, P.J.; Vandenbosch, G.A.E.; Ooi, S.L.; Rais, N.H.M. Design of a Broadband All-Textile Slotted PIFA. *IEEE Trans. Antennas Propag.* **2012**, *60*, 379–384. [CrossRef]
32. Simorangkir, R.B.V.B.; Yang, Y.; Matekovits, L.; Esselle, K.P. Dual-Band Dual-Mode Textile Antenna on PDMS Substrate for Body-Centric Communications. *IEEE Antennas Wirel. Propag. Lett.* **2017**, *16*, 677–680. [CrossRef]
33. Depret, D.; Rogier, H.; Dhaenens, K.; Vanfleteren, J. Flexible-substrate low-cost construction of a coplanar-waveguide aperture-coupled microstrip patch antenna. *Microw. Opt. Technol. Lett.* **2007**, *49*, 1071–1074. [CrossRef]

34. Lorenz, C.H.P.; Hemour, S.; Wu, K. Physical Mechanism and Theoretical Foundation of Ambient RF Power Harvesting Using Zero-Bias Diodes. *IEEE Trans. Microw. Theory Tech.* **2016**, *64*, 2146–2158. [CrossRef]
35. Sun, H.; Geyi, W. A New Rectenna with All-Polarization-Receiving Capability for Wireless Power Transmission. *IEEE Antennas Wirel. Propag. Lett.* **2016**, *15*, 814–817. [CrossRef]